

A Single-Particle Diagnosis of an Interacting Topological Insulator

Théo N. Dionne^{1,2,*} and Maia G. Vergniory^{1,3,2}

¹*Département de Physique et Institut Quantique,*

Université de Sherbrooke, Sherbrooke, J1K 2R1 Québec, Canada

²*Regroupement Québécois sur les Matériaux de Pointe (RQMP), Québec, Canada*

³*Donostia International Physics Center (DIPC), Donostia-San Sebastián, Spain*

(Dated: March 13, 2026)

Understanding how topology survives in strongly correlated systems remains a central challenge, as most topological diagnostics rely on non-interacting band structures. Here we present a framework to characterize interacting topological phases within an effective single-particle description derived from the single-particle Green’s function. Using the Su-Schrieffer-Heeger model with Hatsugai-Kohmoto interactions as an analytically tractable example, we construct the one-body reduced density matrix from the Green’s function and use it to define an effective winding number together with quantum volume, a measurement of state geometry. These quantities allow us to distinguish three insulating phases including correlated Mott states directly from single-particle observables. Our results show that interacting topology can be interpreted in terms of the spectral weight distribution of single-particle excitations, providing an intuitive and computationally accessible route to diagnose topological phases in correlated systems. This approach is compatible with modern many-body simulation techniques and opens a pathway toward the identification of interacting topological materials.

I. INTRODUCTION

The concept of topological phases quickly evolved from early theoretical proposals to the prediction of two-dimensional topological insulators [1, 2], which were experimentally realized shortly thereafter [3–5], and later extended to three-dimensional systems [6–9]. These materials host conducting boundary states protected by symmetries such as time-reversal or crystalline symmetries, forming the class of symmetry-protected topological (SPT) phases characterized by a gapped bulk and robust edge or surface excitations [10–13]. Although the theoretical classification of non-interacting topological phases is now well established, the identification of correlated topological materials has progressed more slowly. A central difficulty has been the lack of a unified framework capable of incorporating crystalline symmetries into topological classification in a way that directly connects abstract theoretical schemes with concrete materials predictions.

The role of strong electronic correlations in topological phases has therefore attracted significant attention [14–16]. In the non-interacting limit, powerful tools such as Topological Quantum Chemistry (TQC) [17] and symmetry indicators [18–20] enable systematic classification of crystalline topology. However, these approaches remain fundamentally rooted in band theory and do not directly extend to interacting systems. In interacting materials, the single-particle Green’s function provides the natural descriptor of electronic structure. Early efforts to incorporate interactions into topological classification include the “topological Hamiltonian” construction [21–23] and approaches based on the zeros of the

Green’s function, which offered valuable insights but remained limited in scope [24, 25]. More recently, proposals to extend TQC using real-space invariants, many-body Green’s functions, and generalized Wannier functions [26–28] have opened promising conceptual directions, although their application to realistic materials remains challenging.

Consequently, diagnosing topology in strongly correlated systems still lacks simple, material-agnostic approaches compatible with modern numerical simulations. In this work we address this problem by studying an analytically solvable extension [29, 30] of the Su-Schrieffer-Heeger model [31] with Hatsugai-Kohmoto interactions [32]. This model provides a controlled setting in which correlation effects can be incorporated while retaining analytic access to the single-particle Green’s function. We analyze the insulating phases that arise in this system directly at the level of the Green’s function [33], which encodes the spectral properties and distribution of single-particle weight and is naturally obtained in many-body numerical methods [34]. From it we construct an effective single-particle description that enables the topology of the interacting phases to be diagnosed through an effective winding number together with a geometric measure of volume in state space, the *quantum volume*. This framework provides a simple route to identifying interacting topological phases using quantities accessible in standard numerical calculations.

II. THEORY

In this section we introduce the theoretical framework used throughout this work. We begin by reviewing single-particle probes in many-body systems and then discuss the geometry of the resulting density matrices. Together

* theo.nathaniel.dionne@usherbrooke.ca

these ideas define what we refer to as the *interacting single particle picture*.

A central object for describing interacting electronic systems is the zero-temperature Green's function, which characterizes the propagation of single-particle excitations in the many-body ground state. It is defined as [35, 36]

$$G_{\mu\nu}(z) = \left\langle \hat{c}_\mu \frac{\mathbb{1}}{z - \hat{H} + E_\Omega} \hat{c}_\nu^\dagger + \hat{c}_\nu^\dagger \frac{\mathbb{1}}{z + \hat{H} - E_\Omega} \hat{c}_\mu \right\rangle \quad (1)$$

where $\hat{c}_\mu^{(\dagger)}$ are the ladder operators associated with the degree of freedom μ . The full information contained in the propagator can be expressed through the spectral function [35]

$$G_{\mu\nu}(z) = \int_{-\infty}^{+\infty} \frac{d\omega}{2\pi} \frac{A_{\mu\nu}(\omega)}{z - \omega}, \quad (2)$$

which encodes the distribution of single-particle spectral weight. The spectral function itself can be obtained from the discontinuity of the Green's function across the real axis,

$$A_{\mu\nu}(\omega) = i [G_{\mu\nu}(\omega + i0^+) - G_{\mu\nu}(\omega - i0^+)]. \quad (3)$$

While the Green's function provides a dynamical description of the system, static single-particle information can be obtained from the one-body reduced density matrix (1RDM). The 1RDM is defined by tracing the full many-body density matrix over all but one particle and can be written as [37, 38]

$$\gamma_{\mu\nu} = \langle \mu | \text{Tr}_{N-1} [\hat{\rho}^N] | \nu \rangle = \langle \hat{c}_\nu^\dagger \hat{c}_\mu \rangle. \quad (4)$$

Because this quantity corresponds to the expectation value of a fermionic bilinear operator, it can be computed directly from the Green's function, and therefore from the spectral function [33, 35, 36]

$$\gamma_{\mu\nu} = \int_{\mathcal{C}_<} \frac{dz}{2\pi i} G_{\mu\nu}(z) = \int_{-\infty}^{\mu} \frac{d\omega}{2\pi} A_{\mu\nu}(\omega). \quad (5)$$

In interacting systems the 1RDM is generally a mixed state, providing an effective description of the equilibrium single-particle physics of the interacting problem in terms of a weighted ensemble of single-particle states.

Once the 1RDM is obtained, its geometric properties across momentum space can be analyzed. Within the interacting single particle picture, topology is encoded in the family of density matrices $\gamma(k)$ defined over the Brillouin zone. From these objects we construct quantities that act as proxies for topological invariants.

The first quantity is an effective winding number $\mathcal{N}_{\text{1RDM}}$, obtained by averaging the Wilczek-Zee connection \mathcal{A} [39] (see Appendix A) in a manner similar to the approach of Ref. [40]. Explicitly,

$$\mathcal{N}_{\text{1RDM}} = \int_{-\pi}^{\pi} \frac{dk}{\pi} \text{Tr} (\mathcal{A}(k) \gamma(k)) \quad (6)$$

A complementary geometric quantity is the quantum volume \mathcal{V} , defined as the volume of the trajectory traced by the density matrices $\gamma(k)$ in the space of density matrices (see Appendix A). In the Fourier-transformed orbital basis this expression reduces to

$$\mathcal{V} = \int_{-\pi}^{\pi} dk \sqrt{\frac{1}{2} \text{Tr} (\partial_k \gamma \partial_k \gamma)} \quad (7)$$

III. MODEL

We consider the Su-Schrieffer-Heeger (SSH) model [31] supplemented by a Hatsugai-Kohmoto (HK) interaction [32], following the approach of Refs. [29, 30]. The SSH lattice consists of two sites per unit cell, labeled *A* and *B*, connected by alternating intra- and inter-cell hopping amplitudes v and w . In addition to the hopping processes, the model includes a momentum-local HK interaction with strength U . A schematic representation of the model is shown in Fig. 1.

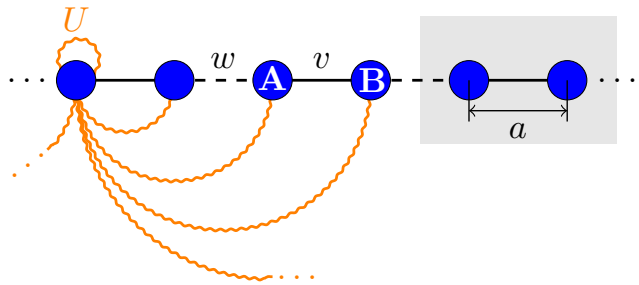


Figure 1: Schematic of the SSH model with HK interactions. The two sites of the unit cell (blue) are labeled *A* and *B*. Nearest neighbours separated by a distance a are connected by intra- and inter-cell hopping amplitudes v and w , respectively. The additional HK interaction of strength U acting between all momentum states is illustrated by the orange wavy lines.

Due to the structure of the HK interaction, the interacting Hamiltonian remains diagonal in reciprocal space [29, 30] (see Appendix B) and can be written as

$$\hat{H} = \sum_{k,a,\sigma} \varepsilon_{k,a} \hat{n}_{k,a,\sigma} + U \sum_k \hat{n}_{k\uparrow} \hat{n}_{k\downarrow}, \quad (8)$$

where k denotes the crystal momentum, a the band index, and σ the spin of the electron. The invariance of the HK interaction in orbital space ensures that the interaction depends only on the total occupation $\hat{n}_{k,\sigma} = \sum_a \hat{n}_{k,a,\sigma}$ [30].

Before considering interactions, it is useful to recall the topology of the non-interacting SSH model. The system is topologically trivial for $w < v$ and topological for $w > v$ [31] (see Appendix C). This classification can also be understood from the inversion symmetry of the lattice,

which is centered in the middle of the unit cell (Fig. 1). At the inversion-invariant momenta $\Gamma = 0$ and $X = \pi/2a$, the Bloch states carry well-defined inversion eigenvalues. In the trivial phase, the lower (upper) band has negative (positive) eigenvalues at both high-symmetry points, whereas in the topological phase the eigenvalues at the X point are reversed.

The diagonal structure of the Hamiltonian allows the ground state to be determined analytically using simple energetic arguments [30] (see Appendix D). The phase diagram can be expressed in terms of a few characteristics of the non-interacting band structure—the bandwidth (BW), the band gap (Δ), and the total width of the spectrum (TW)—together with the interaction strength U and the filling ν . In this work we focus on three insulating regimes:

1. Band insulator with interaction (**BI+U**) at $\nu = 1/2$ and $U < \Delta$,
2. Half-filled Mott insulator (**HFMI**) at $\nu = 1/2$ and $U > \text{TW}$,
3. Quarter-filled Mott insulator (**QFMI**) at $\nu = 1/4$ and $U > \text{BW}$.

The corresponding ground states are summarized in Table I.

Phase	Ground States
BI+U	$\prod_k \hat{c}_{k-\uparrow}^\dagger \hat{c}_{k-\downarrow}^\dagger 0\rangle$
HFMI	$\left\{ \prod_k \hat{c}_{k+\varsigma_k}^\dagger \hat{c}_{k-\varsigma_k}^\dagger 0\rangle \right\}_{\varsigma \in \text{Per}(\sigma)}$
QFMI	$\left\{ \prod_k \hat{c}_{k-\varsigma_k}^\dagger 0\rangle \right\}_{\varsigma \in \text{Per}(\sigma)}$

Table I: Ground states of the SSH+HK model considered in this work.

For these phases the Green's functions can be computed exactly (Appendix E). Their pole structures are illustrated in Fig. 2, where the spectral weight associated with the lower and upper non-interacting bands is indicated in blue and red, respectively. These spectral functions determine the corresponding one-body reduced density matrices, which are summarized in Table II.

Phase	1RDM
BI+U	$ k, -, \sigma\rangle\langle k, -, \sigma $
HFMI	$\frac{1}{2} k, -, \sigma\rangle\langle k, -, \sigma + \frac{1}{2} k, +, \sigma\rangle\langle k, +, \sigma $
QFMI	$\frac{1}{2} k, -, \sigma\rangle\langle k, -, \sigma $

Table II: 1RDMs of the SSH+HK model considered in this work in the basis of non-interacting eigenstates.

The non-interacting eigenstates entering these expres-

sions take the form (see Appendix B)

$$|k, \pm, \sigma\rangle = \frac{1}{\sqrt{2}} \left[\pm e^{i\phi(k)} |k, A, \sigma\rangle + |k, B, \sigma\rangle \right] \quad (9)$$

with

$$\phi(k) = \arctan\left(\frac{w \sin(k2a)}{v + w \cos(k2a)}\right). \quad (10)$$

IV. RESULTS AND DISCUSSION

Here, we analyze the topology and geometry of the SSH+HK model through the lens of the interacting single particle picture. On one hand, the topological contribution at this level is analyzed through an effective winding number. On the other hand, the quantum volume serves as a simple measure of the intrinsic geometry of the 1RDMs.

A. Winding Number

The 1RDM winding numbers (6) for BI+U, HFMI and QFMI as a function of the inter-cell hopping are presented in figure 3. It can be seen that the winding number for both BI+U and QFMI become nonzero when $w > v$, i.e. when the non-interacting model is topological. Moreover, the winding number of the QFMI is half of the one obtained for the BI+U. Conversely, the HFMI retains a trivial winding number. These results correspond well with [29].

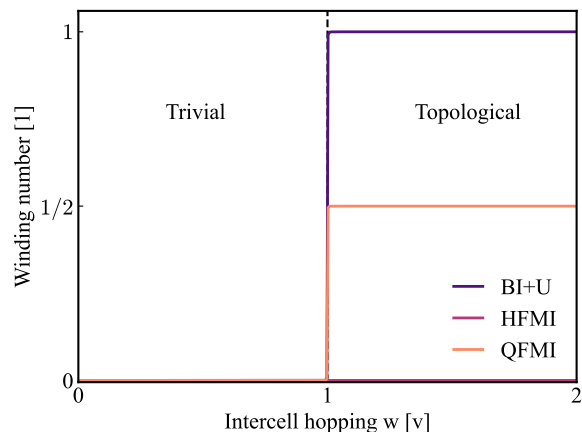


Figure 3: Effective winding number for the three phases studied in the model as a function of the inter-cell hopping w .

These differences may be interpreted by examining the ground states I and the associated 1RDMs II. First, the BI+U is identical to the non-interacting case and hence retains its topological characteristics. Second, the HFMI

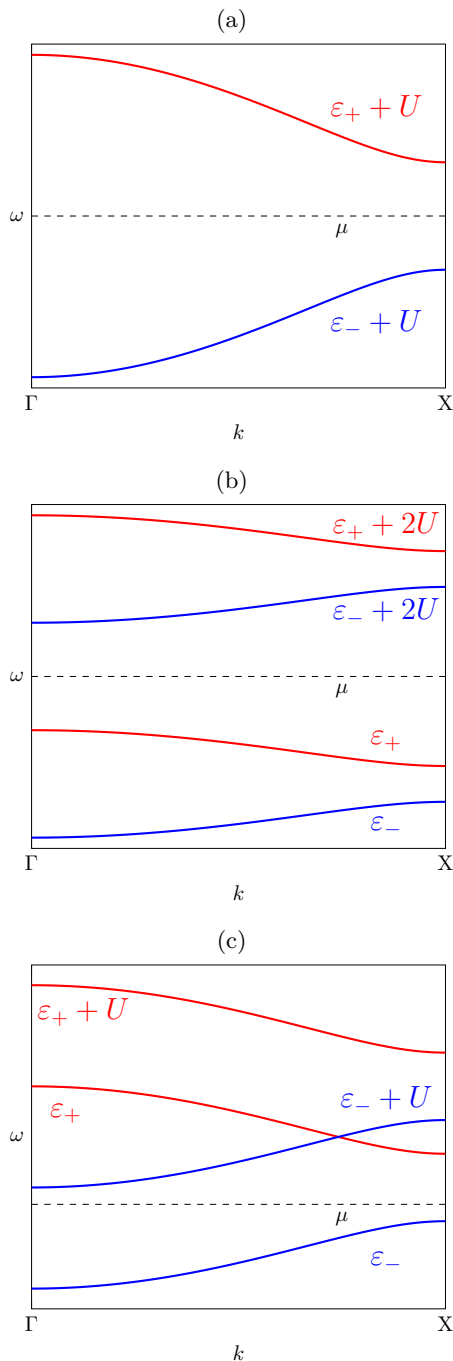


Figure 2: Graphical representations of the spectral functions where blue(red) indicates a relation to the lower(upper) band in the non-interacting model. The chemical potential calculated from the filling is indicated with the dashed line. (a) BI+U. (b) HFMI. (c) QFMI.

contains contributions of equal magnitude and opposite sign from both non-interacting bands, hence one wouldn't expect the phase to have any topology on the interacting single-particle level. Finally, the QFMI is only comprised

of a half-weighted contribution from the lower band.

Additionally, an analogous interpretation is obtained by instead considering the spectral functions **2** of all three phases. What is more transparent when looking at the spectral functions is the possibility of an “effective band inversion”. Indeed, the inversion symmetric properties of the non-interacting model carry over to the spectral function (see **III**). In particular, looking across the chemical potential: the BI+U has full band inversion (fig. **2a**); the HFMI has none (fig. **2b**) while the QFMI has half of an effective band inversion given the single lower-like band under the chemical potential (fig. **2c**).

It should be noted that the plateau-like behaviour of the winding number in this model is directly inherited from the winding number in the non-interacting case, as it is simply related in the case of HK interactions (appendix **A**). In general, this approach seems to “soften” topological invariants [40].

B. Quantum Volume

The quantum volumes for BI+U, HFMI and QFMI as a function of the inter-cell hopping are presented in figure **4**. While the HFMI's quantum volume is fixed at 0 for all parameters, the quantum volume for the BI+U and QFMI steadily increases as a function of w until it attains a constant volume for $w > v$.

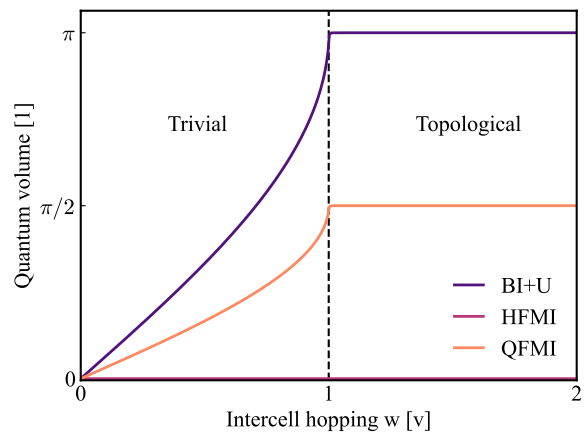


Figure 4: 1RDM quantum volumes for the three phases studied in the model as a function of the inter-cell hopping w .

These traces can be interpreted by referring to the respective 1RDMs (tab. **II**). The quantum volume of the QFMI is always half of the BI+U since the 1RDM is also exactly half. Conversely, since the 1RDM of the HFMI is a multiple of the identity, the target space is that of a point (the identity matrix) and hence is of no volume.

Furthermore, the evolution of the quantum volume as a function of w can be clearly interpreted by inspecting the lower eigenstate (9) of the non-interacting model with which both non-trivial 1RDMs are constructed. At $w =$

0, the lower eigenstate is identical in structure for all k . However, as w is increased, the eigenstate visits more of the ray space of non-interacting states as the phase $\phi(k)$ (10) covers more of the possible angles. It is only at $w > v$ that the phase visits all phase angles. Yet, as w is increased beyond the transition point, the ring-like domain of $\phi(k)$ cannot be expanded further. Hence, the target space of density matrices remains the same, although *parametrized* differently, leaving the volume of this manifold invariant.

V. CONCLUSIONS

In this work, we showed that the SSH+HK model, a topological insulator with long-range interactions, can be characterized at the level of single-particle Green's functions, expanding on previous work [33]. Specifically, the effective one-body winding number reveals the presence of topological phases in the model while the quantum volume gives a different method by which non-trivial topology can be probed. Moreover, the classification of spectral weight at high symmetry-points under inversion

symmetry suggests the possibility of an “effective compatibility relation” which could allow for the diagnosis of interacting topology on the basis of symmetry.

It must be noted that the Hatsugai-Kohmoto interaction cannot be seen as a direct proxy for Coulomb interactions. Hence, the applicability of this method to realistic models is the subject of ongoing work.

ACKNOWLEDGMENTS

We wish to thank André-Marie Tremblay for interesting discussions and helpful suggestions in the writing of this manuscript.

T.N.D. acknowledges the support of the Natural Sciences and Engineering Research Council of Canada (NSERC), the Fonds de recherche du Québec - Nature et technologies (FRQNT) and the Fondation de l'Université de Sherbrooke (FUS).

M.G.V. acknowledges the Canada Excellence Research Chairs Program for Topological Quantum Matter and the support of PID2022-142008NB-I00 funded by MICIU/AEI/10.13039/501100011033 and FEDER, UE.

-
- [1] C. L. Kane and E. J. Mele, Quantum spin hall effect in graphene, *Physical Review Letters* **95**, 226801 (2005).
 - [2] B. A. Bernevig, T. L. Hughes, and S.-C. Zhang, Quantum spin hall effect and topological phase transition in hgte quantum wells, *Science* **314**, 1757 (2006).
 - [3] M. König, S. Wiedmann, C. Brüne, A. Roth, H. Buhmann, L. W. Molenkamp, X.-L. Qi, and S.-C. Zhang, Quantum spin hall insulator state in hgte quantum wells, *Science* **318**, 766 (2007).
 - [4] D. Hsieh, D. Qian, L. Wray, Y. Xia, Y. S. Hor, R. J. Cava, and M. Z. Hasan, A topological dirac insulator in a quantum spin hall phase, *Nature* **452**, 970 (2008).
 - [5] Y. Xia, D. Qian, D. Hsieh, L. Wray, A. Pal, H. Lin, A. Bansil, D. Grauer, Y. S. Hor, R. J. Cava, and M. Z. Hasan, Observation of a large-gap topological-insulator class with a single dirac cone on the surface, *Nature Physics* **5**, 398 (2009).
 - [6] H. Zhang, C.-X. Liu, X.-L. Qi, X. Dai, Z. Fang, and S.-C. Zhang, Topological insulators in bi_2se_3 , bi_2te_3 and sb_2te_3 with a single dirac cone on the surface, *Nature Physics* **5**, 438 (2009).
 - [7] Y. L. Chen, J. G. Analytis, J.-H. Chu, Z. K. Liu, S.-K. Mo, X.-L. Qi, H. J. Zhang, D. H. Lu, X. Dai, Z. Fang, S.-C. Zhang, Z. Hussain, I. R. Fisher, and Z.-X. Shen, Experimental realization of a three-dimensional topological insulator, bi_2te_3 , *Science* **325**, 178 (2009).
 - [8] L. Fu, C. L. Kane, and E. J. Mele, Topological insulators in three dimensions, *Physical Review Letters* **98**, 106803 (2007).
 - [9] M. Z. Hasan and C. L. Kane, Colloquium: Topological insulators, *Reviews of Modern Physics* **82**, 3045 (2010).
 - [10] X.-L. Qi and S.-C. Zhang, Topological insulators and superconductors, *Reviews of Modern Physics* **83**, 1057 (2011).
 - [11] X. Chen, Z.-C. Gu, Z.-X. Liu, and X.-G. Wen, Symmetry-protected topological orders in interacting bosonic systems, *Science* **338**, 1604 (2012).
 - [12] T. Senthil, Symmetry-protected topological phases of quantum matter, *Annu. Rev. Condens. Matter Phys.* **6**, 299 (2015).
 - [13] F. Pollmann, A. M. Turner, E. Berg, and M. Oshikawa, Symmetry protection of topological phases in one-dimensional quantum spin systems, *Phys. Rev. B* **85**, 075125 (2012).
 - [14] S. Rachel, Interacting topological insulators: a review, *Reports on Progress in Physics* **81**, 116501 (2018).
 - [15] D. A. Pesin and L. Balents, Mott physics and band topology in materials with strong spin-orbit interaction, *Nat. Phys.* **6**, 376 (2010).
 - [16] Z. Song, Z. Wang, W. Shi, G. Li, C. Fang, and B. A. Bernevig, All magic angles in twisted bilayer graphene are topological, *Phys. Rev. Lett.* **123**, 036401 (2019).
 - [17] B. Bradlyn, L. Elcoro, J. Cano, M. G. Vergniory, Z. Wang, C. Felser, M. I. Aroyo, and B. A. Bernevig, Topological quantum chemistry, *Nature* **547**, 298 (2017).
 - [18] H. C. Po, A. Vishwanath, and H. Watanabe, Erratum: Symmetry-based indicators of band topology in the 230 space groups, *Nat. Commun.* **8**, 931 (2017).
 - [19] Z. Song, T. Zhang, Z. Fang, and C. Fang, Quantitative mappings between symmetry and topology in solids, *Nat. Commun.* **9**, 3530 (2018).
 - [20] J. Kruthoff, J. de Boer, J. van Wezel, C. L. Kane, and R.-J. Slager, Topological classification of crystalline insulators through band structure combinatorics, *Phys. Rev. X* **7**, 041069 (2017).
 - [21] G. E. Volovik, Topological invariants for standard model: From semimetal to topological insulator, *Phys. Usp.* **61**, 89 (2018).

- [22] M. Iraola, N. Heinsdorf, A. Tiwari, D. Lessnich, T. Mertz, F. Ferrari, M. H. Fischer, S. M. Winter, F. Pollmann, T. Neupert, R. Valentí, and M. G. Vergniory, Towards a topological quantum chemistry description of correlated systems: The case of the hubbard diamond chain, *Phys. Rev. B* **104**, 195125 (2021).
- [23] D. Lessnich, S. M. Winter, M. Iraola, M. G. Vergniory, and R. Valentí, Elementary band representations for the single-particle green's function of interacting topological insulators, *Phys. Rev. B* **104**, 085116 (2021).
- [24] N. Wagner, L. Crippa, A. Amaricci, P. Hansmann, M. Klett, E. J. König, T. Schäfer, D. Di Sante, J. Cano, A. J. Millis, A. Georges, and G. Sangiovanni, Mott insulators with boundary zeros, *Nat. Commun.* **14**, 7531 (2023).
- [25] C. Setty, S. Sur, L. Chen, F. Xie, H. Hu, S. Paschen, J. Cano, and Q. Si, Symmetry constraints and spectral crossing in a mott insulator with green's function zeros, *Phys. Rev. Res.* **6**, L032018 (2024).
- [26] M. O. Soldini, N. Astrakhantsev, M. Iraola, A. Tiwari, M. H. Fischer, R. Valentí, M. G. Vergniory, G. Wagner, and T. Neupert, Interacting topological quantum chemistry of Mott atomic limits, *Physical Review B* **107**, 245145 (2023).
- [27] J. Herzog-Arbeitman, B. A. Bernevig, and Z.-D. Song, Interacting topological quantum chemistry in 2d with many-body real space invariants, *Nat. Commun.* **15**, 1171 (2024).
- [28] B. Monsen and M. Claassen, *Supercell wannier functions and emergent kondo lattices in topological bands* (2024), [arXiv:2412.17190 \[cond-mat.str-el\]](https://arxiv.org/abs/2412.17190).
- [29] S. Mohamadi and J. Abouie, Emergence of topological non-fermi liquid phases in a modified su-schrieffer-heeger chain with long-range interactions, *Physical Review B* **111**, 165129 (2025).
- [30] J. Zhao, P. Mai, B. Bradlyn, and P. Phillips, Failure of topological invariants in strongly correlated matter, *Physical Review Letters* **131**, 106601 (2023), 2305.02341 [cond-mat].
- [31] W. P. Su, J. R. Schrieffer, and A. J. Heeger, Solitons in polyacetylene, *Phys. Rev. Lett.* **42**, 1698 (1979).
- [32] Y. Hatsugai and M. Kohmoto, Exactly solvable model of correlated lattice electrons in any dimensions, *Journal of the Physical Society of Japan* **61**, 2056 (1992).
- [33] T. N. Dionne, S. Villodre, M. Iraola, and M. G. Vergniory, *Characterizing mott insulators in the interacting one-body picture* (2026), [arXiv:2511.07331 \[cond-mat.str-el\]](https://arxiv.org/abs/2511.07331).
- [34] D. Sénéchal, A.-M. Tremblay, and C. Bourbonnais, *Theoretical methods for strongly correlated electrons* (Springer Science & Business Media, 2004).
- [35] G. Rickayzen, *Green's Functions and Condensed Matter*, Materials Science Series (Academic Press, 1980).
- [36] T. N. Dionne, A. Foley, M. Rousseau, and D. Sénéchal, Pyqcm: An open-source Python library for quantum cluster methods, *SciPost Phys. Codebases* , 23 (2023).
- [37] J. P. Solovej, Many body quantum mechanics, *Notes* (2007).
- [38] E. Gross, E. Runge, and O. Heinonen, *Many-Particle Theory*, (Taylor & Francis, 1991).
- [39] F. Wilczek and A. Zee, Appearance of gauge structure in simple dynamical systems, *Phys. Rev. Lett.* **52**, 2111 (1984).
- [40] X. Wang, X.-Y. Hou, Y. He, and H. Guo, *Thermal Uhlmann-Chern Number: Bridging Pure and Mixed States* (2025), [arXiv:2506.18022 \[quant-ph\]](https://arxiv.org/abs/2506.18022).
- [41] Z. Wang, X.-L. Qi, and S.-C. Zhang, Topological order parameters for interacting topological insulators, *Phys. Rev. Lett.* **105**, 256803 (2010).
- [42] Z. Wang and S.-C. Zhang, Simplified topological invariants for interacting insulators, *Phys. Rev. X* **2**, 031008 (2012).
- [43] P. Mai, J. Zhao, B. E. Feldman, and P. W. Phillips, 1/4 is the new 1/2 when topology is intertwined with mottness, *Nat Commun* **14**, 5999 (2023), publisher: Nature Publishing Group.
- [44] M. Zhao, W.-W. Yang, and Y. Zhong, Hatsugai–kohmoto models: exactly solvable playground for mottness and non-fermi liquid, *Journal of Physics: Condensed Matter* **37**, 183005 (2025).
- [45] K. Jabłonowski, J. Skolimowski, W. Brzezicki, K. Byczuk, and M. M. Wysokiński, Topological mott insulator in the odd-integer filled anderson lattice model with hatsugai-kohmoto interactions, *Phys. Rev. B* **108**, 195145 (2023).
- [46] P. Mai, B. E. Feldman, and P. W. Phillips, Topological mott insulator at quarter filling in the interacting haldane model, *Phys. Rev. Res.* **5**, 013162 (2023).
- [47] R. Cheng, *Quantum geometric tensor (fubini-study metric) in simple quantum system: A pedagogical introduction* (2013), [arXiv:1012.1337 \[quant-ph\]](https://arxiv.org/abs/1012.1337).
- [48] M. Nakahara, *Geometry, topology and physics* (CRC Press, 2003) bristol, UK: Hilger (1990) 505 p. (Graduate student series in physics).
- [49] Y. S. Lyakhova, G. V. Astretsov, and A. N. Rubtsov, Mean-field concept and post-DMFT methods in the modern theory of correlated systems, *Physics-Uspekhi* **66**, 775 (2023).
- [50] N. F. Mott, The basis of the electron theory of metals, with special reference to the transition metals, *Proceedings of the Physical Society. Section A* **62**, 416 (1949).
- [51] G. R. Stewart, Unconventional superconductivity, *Advances in Physics* **66**, 75 (2017), <https://doi.org/10.1080/00018732.2017.1331615>.
- [52] I. I. Lungu, A. M. Grumezescu, and C. Fleaca, Unexpected ferromagnetism—a review, *Applied Sciences* **11**, 6707 (2021).
- [53] M. V. Berry, Quantal phase factors accompanying adiabatic changes, *Proceedings of the Royal Society of London. A. Mathematical and Physical Sciences* **392**, 45 (1984), <https://royalsocietypublishing.org/rspa/article-pdf/392/1802/45/65511/rspa.1984.0023.pdf>.
- [54] D. Chruściński and A. Jamiolkowski, *Geometric Phases in Classical and Quantum Mechanics* (Birkhäuser, 2004).
- [55] E. Fradkin, *Quantum Field Theory: An Integrated Approach* (Princeton University Press, 2021).
- [56] B. Bradlyn and M. Iraola, Lecture notes on Berry phases and topology, *SciPost Phys. Lect. Notes* , 51 (2022).
- [57] E. Cornfeld and S. Carmeli, Tenfold topology of crystals: Unified classification of crystalline topological insulators and superconductors, *Physical Review Research* **3**, 013052 (2021).
- [58] D. M. Neno, C. A. C. Garcia, J. Gooth, C. Felser, and P. Narang, Axion physics in condensed-matter systems, *Nature Reviews Physics* **2**, 682 (2020).
- [59] M. J. Gilbert, Topological electronics, *Communications Physics* **4**, 70 (2021).
- [60] R. Durand, L.-T. Gendron, T. N. Dionne, and I. Garate, Nonlinear longitudinal current of band-geometric origin

in wires of finite thickness, *Phys. Rev. Lett.* **133**, 226302 (2024).

Appendix A: 1RDM geometry and topology

In this appendix, we explicit how topology and geometry are measured on the 1RDM in this work. First, we briefly cover covariant differentiation and show how it implies the appearance of an auxiliary gauge field. Notions of distance in the space of matrices are explained. Then, the 1RDM formulation of the standard winding number is given before defining the notion of a suitable quantum volume.

1. Covariant Differentiation

The 1RDM defines a map between a parameter manifold \mathcal{M} and the space of hermitian positive semi-definite operators \mathcal{D}^+ [56]:

$$\hat{\gamma} : \mathcal{M} \rightarrow \mathcal{D}^+ \quad (\text{A1})$$

These operators can be represented in any orthonormal basis as:

$$\hat{\gamma}(\lambda) = \gamma_{\mu\nu}(\lambda) |\phi_\mu(\lambda)\rangle\langle\phi_\nu(\lambda)| \quad (\text{A2})$$

The derivative of the density operator can be written in terms of components:

$$\langle\phi_\alpha|\partial_t\hat{\gamma}|\phi_\beta\rangle = \partial_t\gamma_{\alpha\beta} - i\mathcal{A}_{\alpha\nu}\gamma_{\nu\beta} + i\gamma_{\alpha\nu}\mathcal{A}_{\nu\beta} \quad (\text{A3})$$

with the non-abelian Wilczek-Zee connection [39] as:

$$\mathcal{A}_{\mu\nu} = i\langle\phi_\mu|\partial_t|\phi_\nu\rangle \quad (\text{A4})$$

Hence, we define the covariant derivative in the coordinate representation as:

$$\mathcal{D}_t\gamma = \partial_t\gamma - i[\mathcal{A}, \gamma] \quad (\text{A5})$$

It can be easily checked that under a change of basis, the covariant derivative of a coordinate matrix transforms as a coordinate matrix [55]

$$\mathcal{D}'_t\gamma' = \mathbf{U}\mathcal{D}_t\gamma\mathbf{U}^\dagger \quad (\text{A6})$$

as long as connection transforms as usual:

$$\mathcal{A}' = \mathbf{U}\mathcal{A}\mathbf{U}^\dagger - i\partial_t(\mathbf{U})\mathbf{U}^\dagger \quad (\text{A7})$$

This connection can be considered as the local connection on a $U(N)$ principle bundle [48, 54].

2. State Metric

What is the notion of distance on the manifold of 1RDMs $\gamma \in \mathcal{D}^+$? In this work, we base ourselves on the Hilbert-Schmidt distance defined for operators as:

$$\left(\hat{A}, \hat{B}\right) = \text{Tr}\left(\hat{A}^\dagger\hat{B}\right) \quad (\text{A8})$$

This can be used to define an infinitesimal distance element or *metric* in the space of 1RDMs. If we take the derivative along a path $\lambda \in \mathcal{B}$, the distance element at each point is

$$ds^2 \propto (\mathcal{D}_\lambda \gamma, \mathcal{D}_\lambda \gamma) d\lambda^2 = \text{Tr} \left[(\mathcal{D}_\lambda \gamma)^\dagger \mathcal{D}_\lambda \gamma \right] d\lambda^2$$

where we have left the possibility for a scaling coefficient. This proportionality is fixed by the pure state limit where the appropriate metric is the Fubini-Study metric (often referred to as the Quantum Geometric Tensor) [47, 48]. To do this, let $\gamma(\lambda) = |\psi(\lambda)\rangle\langle\psi(\lambda)|$ and $\dot{\circ} \equiv \partial_\lambda \circ$. The line element is then:

$$ds^2 = \kappa \text{Tr} (\dot{\gamma}^2) \quad (\text{A9})$$

The quantity in the trace is:

$$\begin{aligned} \dot{\gamma}^2 = & |\dot{\psi}\rangle\langle\psi| \dot{\psi}\rangle\langle\psi| + |\dot{\psi}\rangle\langle\psi| \psi\rangle\langle\dot{\psi}| \\ & + |\psi\rangle\langle\dot{\psi}| \dot{\psi}\rangle\langle\psi| + |\psi\rangle\langle\dot{\psi}| \psi\rangle\langle\dot{\psi}| \end{aligned} \quad (\text{A10})$$

Using the normalization of the state $\langle\psi|\psi\rangle = 1$ to write $\langle\dot{\psi}|\psi\rangle = -\langle\psi|\dot{\psi}\rangle$, we can rewrite the expression as:

$$\begin{aligned} \dot{\gamma}^2 = & -|\dot{\psi}\rangle\langle\dot{\psi}| \psi\rangle\langle\psi| + |\dot{\psi}\rangle\langle\dot{\psi}| \\ & + |\psi\rangle\langle\dot{\psi}| \dot{\psi}\rangle\langle\psi| - |\psi\rangle\langle\dot{\psi}| \psi\rangle\langle\dot{\psi}| \end{aligned} \quad (\text{A11})$$

Hence, upon taking the trace, cyclicity and completeness allow the expression to take the following form:

$$\text{Tr} (\dot{\gamma}^2) = 2 \langle\dot{\psi}| (1 - |\psi\rangle\langle\psi|) |\dot{\psi}\rangle \quad (\text{A12})$$

which is nothing more than a multiple of the Fubini-Study metric on the projective space in the ray-space of physically distinct states [48]. This completely fixes the metric since $\kappa = 1/2$ is required to maintain equality with the FS metric in the pure limit. Define the density operator metric as:

$$g_{\mu\nu}^{(\text{1RDM})} = \frac{1}{2} \text{Tr} (\partial_\mu \gamma \partial_\nu \gamma) \frac{\partial \lambda}{\partial x^\mu} \frac{\partial \lambda}{\partial x^\nu} \quad (\text{A13})$$

such that:

$$ds^2 = g_{\mu\nu} dx^\mu dx^\nu \quad (\text{A14})$$

as it should.

3. Winding Number

In this work, we calculate the winding number of the effective one-body problem by integrating over the averaged gauge field in a way that is similar to what was done in other works, notably [40]. The integral yielding the winding number can thus be written as:

$$\mathcal{N}_{\text{1RDM}} = \int_{-\pi}^{\pi} \frac{dk}{\pi} \text{Tr} (\mathcal{A}(k) \bar{\gamma}(k)) \quad (\text{A15})$$

Being diagonal in the non-interacting band basis of the model, $\hat{\gamma} = p_+ |k, +\rangle\langle k, +| + p_- |k, -\rangle\langle k, -|$, hence yielding a pleasant form:

$$\mathcal{N}_{\text{1RDM}} = p_+ \mathcal{N}_+ + p_- \mathcal{N}_- \quad (\text{A16})$$

which is only possible due to the k -diagonal nature of the model. It should be noted that this reduces exactly to the standard winding number when there are no interactions, i.e. $N_{\text{1RDM}} = N_-$, which is to be expected since the interacting single particle picture coincides with the band picture in the absence of interactions.

4. Quantum Volume

The volume of the target space of density matrices is simple to calculate in the fixed orbital basis since the connection vanishes $\mathcal{A} = \mathbf{0}$ implying that the covariant derivative reduces to an ordinary derivative. The integral yielding the volume of the space is constructed from the suitable metric (A13):

$$\mathcal{V} = \int_{-\pi}^{\pi} dk \sqrt{\frac{1}{2} \text{Tr} (\partial_k \gamma \partial_k \gamma)} \quad (\text{A17})$$

Appendix B: Construction of the model

In this appendix, the model (figure 1) is explicitly constructed and diagonalized in reciprocal space and band space.

In real space, the Hamiltonian can be read from the graphical representation of the model 1:

$$\begin{aligned} \hat{H} = & - \sum_{i\sigma} \left[v \hat{c}_{i,B,\sigma}^\dagger \hat{c}_{i,A,\sigma} + w \hat{c}_{i+1,A,\sigma}^\dagger \hat{c}_{i,B,\sigma} + \text{h.c.} \right] \\ & + U \sum_{ij} (\hat{n}_{i,A,\uparrow} + \hat{n}_{i,B,\uparrow}) (\hat{n}_{j,A,\downarrow} + \hat{n}_{j,B,\downarrow}) \end{aligned} \quad (\text{B1})$$

where $v, w, U \in \mathbb{R}^+$, $\hat{c}_{i,s,\sigma}^{(\dagger)}$ annihilates(creates) an electron at site s of cell i with spin σ and $\hat{n} = \hat{c}^\dagger \hat{c}$. The following convention for Fourier transforms,

$$\hat{c}_{k,s,\sigma} = \frac{1}{\sqrt{N}} \sum_j e^{-ik(2a)j} \hat{c}_{j,s,\sigma} \quad (\text{B2})$$

$$\hat{c}_{j,s,\sigma} = \frac{1}{\sqrt{N}} \sum_k e^{+ik(2a)j} \hat{c}_{k,s,\sigma} \quad (\text{B3})$$

is used to rewrite the Hamiltonian in reciprocal space:

$$\begin{aligned} \hat{H} = & - \sum_{k\sigma} \left[v \hat{c}_{k,B,\sigma}^\dagger \hat{c}_{k,A,\sigma} + w e^{-ik2a} \hat{c}_{k,A,\sigma}^\dagger \hat{c}_{k,B,\sigma} + \text{h.c.} \right] \\ & + U \sum_k (\hat{n}_{k,A,\uparrow} + \hat{n}_{k,B,\uparrow}) (\hat{n}_{k,A,\downarrow} + \hat{n}_{k,B,\downarrow}) \end{aligned} \quad (\text{B4})$$

The Hamiltonian can now be rendered fully diagonal,

$$\hat{H} = \sum_{k,a,\sigma} \varepsilon_{k,a,\sigma} \hat{n}_{k,a,\sigma} + U \sum_k \hat{n}_{k\uparrow} \hat{n}_{k\downarrow} \quad (\text{B5})$$

by using the eigenmodes of the non-interacting part

$$\hat{c}_{k,\pm,\sigma}^\dagger = \frac{1}{\sqrt{2}} \left[\pm e^{i\phi(k)} \hat{c}_{k,A,\sigma}^\dagger + \hat{c}_{k,B,\sigma}^\dagger \right] \quad (\text{B6})$$

where

$$\phi(k) = \arctan\left(\frac{w \sin(k2a)}{v + w \cos(k2a)}\right) \quad (\text{B7})$$

along with the associated eigenenergies of the non-interacting portion:

$$\varepsilon_{k,\pm,\sigma} = \sqrt{v^2 + w^2 + 2vw \cos(2ka)} \quad (\text{B8})$$

Appendix C: Topology and symmetry of the non-interacting SSH model

In this appendix, the topology and inversion symmetric properties of the non-interacting Hamiltonian are red-erived.

On one hand, it is well known [31] that the SSH model is trivial for $w < v$ and topological for $v > w$. This topology is assessed by calculating the winding numbers associated with the bands of the model:

$$\mathcal{N}_\pm = \int_{-\pi}^{\pi} \frac{dk}{\pi} A_\pm(k) = \begin{cases} 0, & w < v \\ \mp 1, & w > v \end{cases} \quad (\text{C1})$$

where $A_\pm(k) = i \langle k, \pm | \partial_k | k, \pm \rangle$ is the Berry connection [53] of the \pm band.

On the other hand, the model possesses inversion symmetry as defined by $j \mapsto -j$ and $A(B) \mapsto B(A)$. Note that spin is safely ignored because of the spin-invariance of the model.

In reciprocal space, these properties are reflected in the high symmetry points $\Gamma = 0$ and $X = \pi/2a$ which are invariant under inversion $k \rightarrow -k$. Given the invariance of the band Hamiltonian under inversion at these points, the corresponding eigenstates may be assigned a parity under inversion. Specifically the non-interacting Hamiltonian at these specific points becomes,

$$H(\Gamma) = \begin{pmatrix} 0 & v+w \\ v+w & 0 \end{pmatrix} \quad (\text{C2})$$

$$H(X) = \begin{pmatrix} 0 & v-w \\ v-w & 0 \end{pmatrix} \quad (\text{C3})$$

The eigenvectors in the orbital basis at the high symmetry points will be of the schematic form $|\pm\rangle = \frac{1}{\sqrt{2}} (\pm|A\rangle + |B\rangle)$ and transform as:

$$|\pm\rangle \xrightarrow{\text{inversion}} \pm |\pm\rangle \quad (\text{C4})$$

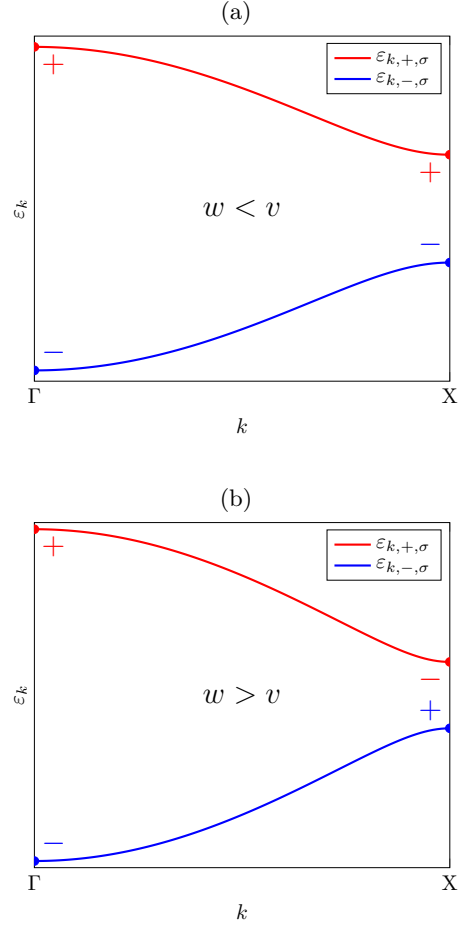


Figure 5: (a) Band structure of \hat{H}_0 for a trivial parameter regime $1 = v > w = 0.5$ where the lower band is entirely comprised of inversion-odd states while the upper band is fully inversion-even. (b) Band structure of \hat{H}_0 for a topological parameter regime $1 = v < w = 1.5$ where the inversion parity of the bands is inverted at X when compared to the trivial phase.

Each state can be assigned a band at the two highlighted points by checking their eigenenergies. At Γ ,

$$H(\Gamma) |\pm\rangle = \begin{cases} 2(v+w) |+\rangle \\ 0 |-\rangle \end{cases} \quad (\text{C5})$$

meaning in conjunction with (C4) that no matter the phase, the upper(lower) band at Γ is always even(odd) under inversion. Conversely, at X,

$$H(X) |\pm\rangle = \begin{cases} 2(v-w) |+\rangle \\ 0 |-\rangle \end{cases} \quad (\text{C6})$$

showing that there is indeed an inversion of parity when the system becomes topological ($w > v$). The band structures with associated parities are represented in figure 5.

Appendix D: Calculation of the ground states

In this appendix, the ground states of the model are derived using simple arguments. First, the two phases identified at half filling ($\nu = 1/2$) are obtained. Then, it is shown that the quarter-filled ($\nu = 1/4$) system can become a Mott insulator in the presence of HK interactions.

The analysis here is predicated on the Hamiltonian (B1). We make use of the fact that the system is block-diagonalized into sectors corresponding to each wavevector in the B.Z.:

$$\hat{H}_k = \varepsilon_{k,+} \hat{n}_{k,+} + \varepsilon_{k,-} \hat{n}_{k,-} + U \hat{n}_{k,\uparrow} \hat{n}_{k,\downarrow} \quad (\text{D1})$$

where missing indices are summed over. It should be noted that we impose that the total spin projection vanishes.

1. Half-Filling

In the absence of interactions, the model is a band insulator at $\nu = 1/2$ with the typical Fermi sea ground state. In this state, each k in the lower band is doubly occupied 6a. As the interaction U is increased, one U contribution from each k is incurred from the density-density interaction. However, as long as the value of the interaction does not exceed the size of the gap (Δ), none of the electrons can lower their energies by tunneling to the upper band. Hence, as long as $U < \Delta$, the ground state is a Fermi sea:

$$|\Omega_{\text{BI}}\rangle = \prod_k \hat{c}_{k-\uparrow}^\dagger \hat{c}_{k-\downarrow}^\dagger |0\rangle \quad (\text{D2})$$

As the interaction is further increased, the k -points for which the interaction exceeds the non-interacting band gap will have one electron in the upper band and one in the lower band. Specifically, this is due to the form of the interactions, since the interacting contribution can be completely avoided by having two electrons with the same spin at the same k -point on the two different bands 6b. This state will be metallic in nature because of the partially filled bands.

Finally, as the interaction strength is raised as to exceed the total band structure width (TW), both bands will be entirely singly occupied with the constraint that the spin at each k -point be of one given variety (figure 6c). Hence, the ground state in this phase is highly degenerate. This set of degenerate ground states can be represented as:

$$\mathcal{H}_0^{\text{HFMI}} = \left\{ \prod_k \hat{c}_{k+\varsigma_k}^\dagger \hat{c}_{k-\varsigma_k}^\dagger |0\rangle \right\}_{\varsigma \in \text{Per}(\sigma)} \quad (\text{D3})$$

where $\text{Per}(\sigma)$ is to be interpreted as the permutations of all half-filled spin configurations.

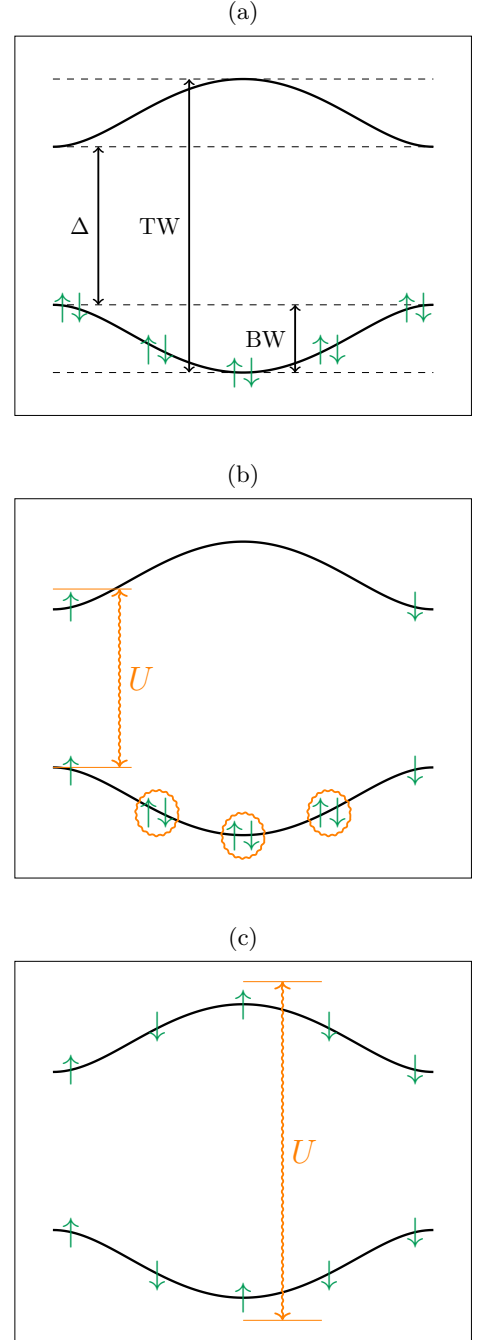


Figure 6: Graphical representations of phases at $\nu = 1/2$. (a) Ground state of the BI+U ($U < \Delta$) along with useful dimensions. (b) Transitional metallic phase(s) between BI+U and HFMI ($\Delta \leq U \leq \text{TW}$). (c) Ground states of the HFMI ($U > \text{TW}$).

2. Quarter-Filling

Conversely, at $\nu = 1/4$, the model is metallic at $U = 0$ as the lower band is half-filled (fig. 7a). As U is in-

creased, the electrons can spread out across the lower band as to avoid some of the energetic cost of double occupancy. However, as U reaches the bandwidth (BW), the least energetic set of states will be those where the electrons are distributed such that the lower band is entirely singly occupied (fig. 7b). The resulting phase can be characterized as a Mott insulator as the metallic nature of the non-interacting system entirely gives way to a correlated insulator. The ground states are also massively degenerate and are labeled as:

$$\mathcal{H}_0^{\text{QFMI}} = \left\{ \prod_k \hat{c}_{k-\zeta_k}^\dagger |0\rangle \right\}_{\zeta \in \text{Per}(\sigma)} \quad (\text{D4})$$

Comparison of either equations (D3) and (D4) or figures 6c and 7b reveal that the QFMI can be seen as effectively ‘half’ of the HFMI.

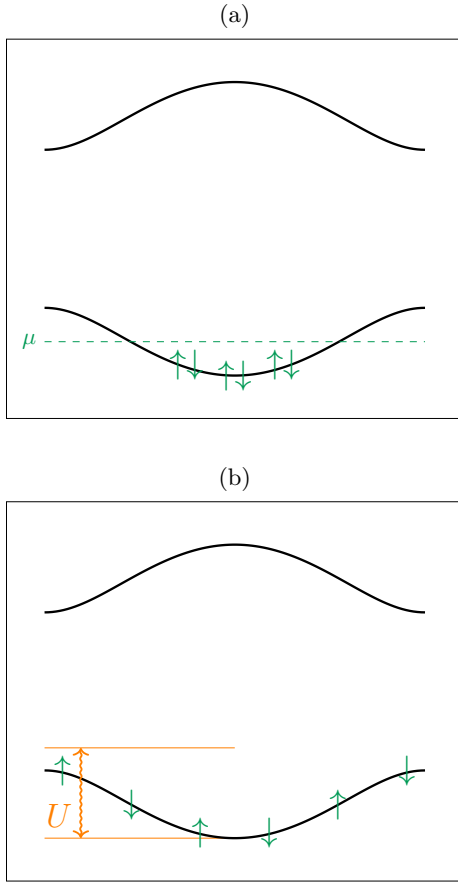


Figure 7: Graphical representations of phases at $\nu = 1/4$. (a) Metallic ground state at quarter filling ($U = 0$). (b) Ground states of the QFMI ($U > \text{BW}$).

Appendix E: Calculation of the Green’s functions

In this appendix, the exact zero temperature Green’s functions for the phases derived in appendix D are calcu-

lated, implying exact solutions for the spectral functions. For a N_Ω -fold degenerate ground state, one can write the zero temperature Green’s function as [35, 36]:

$$G_{n,\sigma}(k, z) = \frac{1}{N_\Omega} \sum_\alpha \langle \Omega_{k;\alpha} | \left\{ \hat{c}_{k,n,\sigma} \frac{\mathbb{1}}{z - \hat{H}_k + E_\Omega} \hat{c}_{k,n,\sigma}^\dagger + \hat{c}_{k,n,\sigma}^\dagger \frac{\mathbb{1}}{z + \hat{H}_k - E_\Omega} \hat{c}_{k,n,\sigma} \right\} | \Omega_{k;\alpha} \rangle \quad (\text{E1})$$

where the diagonal nature in k allows us to simply consider the sector of Hilbert space related to the k -point. In analytical calculations, it is often practical to split the Green’s function into its ‘electron’ and ‘hole’ parts:

$$G_{n,\sigma}^{(e)}(k, z) = \frac{1}{N_\Omega} \sum_\alpha \frac{\langle \Omega_{k;\alpha} | \hat{c}_{k,n,\sigma} \hat{c}_{k,n,\sigma}^\dagger | \Omega_{k;\alpha} \rangle}{z - \hat{H}_k + E_\Omega} \quad (\text{E2})$$

$$G_{n,\sigma}^{(h)}(k, z) = \frac{1}{N_\Omega} \sum_\alpha \frac{\langle \Omega_{k;\alpha} | \hat{c}_{k,n,\sigma}^\dagger \hat{c}_{k,n,\sigma} | \Omega_{k;\alpha} \rangle}{z + \hat{H}_k - E_\Omega} \quad (\text{E3})$$

We call the weights of the poles the overlap, they are defined as:

$$p_{k,n,\sigma;\alpha}^{(e)} \equiv \frac{1}{N_\Omega} \langle \Omega_\alpha(k) | \hat{c}_{k,n,\sigma} \hat{c}_{k,n,\sigma}^\dagger | \Omega_\alpha(k) \rangle \quad (\text{E4})$$

$$p_{k,n,\sigma;\alpha}^{(h)} \equiv \frac{1}{N_\Omega} \langle \Omega_\alpha(k) | \hat{c}_{k,n,\sigma}^\dagger \hat{c}_{k,n,\sigma} | \Omega_\alpha(k) \rangle \quad (\text{E5})$$

$$1 = \sum_\alpha \left(p_{k,n,\sigma;\alpha}^{(e)} + p_{k,n,\sigma;\alpha}^{(h)} \right) \quad (\text{E6})$$

where the last equality holds due to canonical anticommutation. These weights represent the statistical contribution of each ground state to the dynamics. The energy of the excitations are encoded in:

$$E_{k,n,\sigma;\alpha}^{(e)} \equiv \langle \Omega_{k;\alpha} | \hat{c}_{k,n,\sigma} \hat{H}_k \hat{c}_{k,n,\sigma}^\dagger | \Omega_{k;\alpha} \rangle \quad (\text{E7})$$

$$E_{k,n,\sigma;\alpha}^{(h)} \equiv \langle \Omega_{k;\alpha} | \hat{c}_{k,n,\sigma}^\dagger \hat{H}_k \hat{c}_{k,n,\sigma} | \Omega_{k;\alpha} \rangle \quad (\text{E8})$$

All of these quantities can be calculated in a modular fashion and are later recombined into the full Green’s function:

$$G_{n,\sigma}(k, z) = \sum_\alpha \left[\frac{p_{k,n,\sigma;\alpha}^{(e)}}{z - \Delta E_{k,n,\sigma;\alpha}^{(e)}} + \frac{p_{k,n,\sigma;\alpha}^{(h)}}{z - \Delta E_{k,n,\sigma;\alpha}^{(h)}} \right] \quad (\text{E9})$$

which also offers a particularly limpid insight into the structure of the Green’s function.

1. BI+U

At any given k -point, the ground state is expressed as $|- \uparrow - \downarrow \rangle$. The energy of this ground state is simply given by:

$$E_\Omega = 2\varepsilon_{k,-} + U \quad (\text{E10})$$

The electronic part only has a contribution for $n = +$ since the lower band is fully occupied:

$$p_n^{(e)} = \delta_{n,+} \quad (\text{E11})$$

where the energy of the resulting state with an added electron is:

$$E_n^{(e)} = 2\varepsilon_{k,-} + \varepsilon_{k,+} + 2U \quad (\text{E12})$$

Similarly, the hole part only contributes when $n = -$:

$$p_n^{(h)} = \delta_{n,-} \quad (\text{E13})$$

The energy of the resulting state with one removed electron is simply:

$$E_n^{(h)} = \varepsilon_{k,-} \quad (\text{E14})$$

no matter the spin. Hence, we obtain the Green's function for the BI+U phase:

$$G_{n,\sigma}(k, z) = \frac{\delta_{n,+}}{z - (\varepsilon_{k,+} + U)} + \frac{\delta_{n,-}}{z - (\varepsilon_{k,-} + U)} \quad (\text{E15})$$

2. HFMI

The two ground states that must be considered are $\{|+\uparrow-\uparrow\rangle, |+\downarrow-\downarrow\rangle\}$. Focusing first on the overlaps,

$$p_n^{(e)} = \frac{1}{2} = p_n^{(h)} \quad (\text{E16})$$

We may now calculate the relevant energies, starting with the energy of the ground states:

$$E_\Omega = \varepsilon_+ + \varepsilon_- \quad (\text{E17})$$

The energies of the electron type excited states is

$$E_n^{(e)} = E_\Omega + \varepsilon_n + 2U \quad (\text{E18})$$

while the energies of the hole like states are

$$E_n^{(h)} = E_\Omega - \varepsilon_n \quad (\text{E19})$$

Such that the total Green's function for HFMI reads:

$$G_{n,\sigma}(k, z) = \frac{\delta_{n,+}}{2} \left[\frac{1}{z - (\varepsilon_{k,+} + 2U)} + \frac{1}{z - \varepsilon_{k,+}} \right] + \frac{\delta_{n,-}}{2} \left[\frac{1}{z - (\varepsilon_{k,-} + 2U)} + \frac{1}{z - \varepsilon_{k,-}} \right] \quad (\text{E20})$$

3. QFMI

In this case, the ground states to consider at each point are $\{|-\uparrow\rangle, |-\downarrow\rangle\}$, which signifies that the relevant overlaps are:

$$p_n^{(e)} = \delta_{n,+} + \frac{\delta_{n,-}}{2} \quad (\text{E21})$$

$$p_n^{(h)} = \frac{\delta_{n,-}}{2} \quad (\text{E22})$$

The ground state energy is simply:

$$E_\Omega = \varepsilon_- \quad (\text{E23})$$

while the excited energies for added and removed particles read as:

$$E_{n,\sigma}^{(e)} = E_\Omega + \varepsilon_n + \delta_{\sigma,-\sigma_{GS}} U \quad (\text{E24})$$

$$E_{-,\sigma}^{(h)} = 0 \quad (\text{E25})$$

Giving the following Green's function:

$$G_{n,\sigma}(k, z) = \frac{\delta_{n,+}}{2} \left[\frac{1}{z - (\varepsilon_{k,+} + U)} + \frac{1}{z - \varepsilon_{k,+}} \right] + \frac{\delta_{n,-}}{2} \left[\frac{1}{z - (\varepsilon_{k,-} + U)} + \frac{1}{z - \varepsilon_{k,-}} \right] \quad (\text{E26})$$